A NOVEL WAY OF CONSTRUCTING NEO-URINARY CONDUIT BY USING DECELLULARIZED TISSUES

by

Chenhao Fang

A thesis submitted to The Johns Hopkins University in conformity with the requirements for the degree of Master of Science in Engineering in: Chemical and Biomolecular Engineering

Baltimore, Maryland

July 2018

Abstract

Biologic scaffolds derived from decellularized tissues and organs have already been successfully used in both pre-clinical animal studies and human clinical applications, so more attentions have been paid to regenerative and medical applications of decellularized tissues. Here, we report a novel way of constructing tissue-engineered conduit by the use of decellularized tissues. For the patients who have bladder cancer, they do need a way to pass urine out of their body when they have the surgery to remove the diseased bladder. A neo-urinary conduit (NUC) is such a man-made organ that can work as a passage for urine removal for those patients in bladder cancer. Considering the naturally biological compositions and excellent mechanical and structural properties, a decellularized trachea must be a fabulous candidate for NUC.

In this paper, we use the decellularized trachea from rabbit and further estimate its mechanical properties and whether it is feasible to grow human smooth muscle cells (hSMCs) and human urothelial cells (hUCs) on it. According to the results of mechanical testing, we found that the decellularized trachea has ultimate tensile strength (UTS) of 0.34 MPa in longitudinal direction and 1.03 MPa in circumferential direction. In addition, the scanning electron microscopy (SEM) results show that in the lumen of the scaffold, hUCs grow in a flatten pattern and are interconnected with each other, while on the outer surfaces, they are round and spherical. For hSMCs, they can penetrate the scaffold and grow anywhere. Also, the results of immunostaining and quantitative RT-PCR indicate the hSMCs are able to grow and survive on the scaffold for a long time, which provides the possibility of applying the scaffold to the clinical studies.

Advisor: Dr. Anirudha Singh

Reader: Dr. Jamie Spangler

Acknowledgements

First, I would like to thank my parents for providing me with the opportunity to attend The Johns Hopkins University. Without their support, love, and numerous sacrifices, I would not have been able to succeed in such a prestigious academic institution. Additionally, I want to thank my friends in China. They have inspired me to push myself beyond my limits and to never give up no matter what happened in life.

Dr. Anirudha Singh-Thank you for accepting me into your lab and giving me the wonderful experience of working with this fascinating biological research. Without inspiration from your class about the fabrication and application of polymers, I may have not considered continuing my research in this field. You have given me invaluable wisdom pertaining to research and life on a lot of occasions, and I will never forget those lessons.

Also, I would like to thank Christine Yu, Jiuru Li and Harrison Jeong for mentoring me throughout the past two years. You taught me everything I needed to know to operate the equipment in the lab and helped me organize and carry out the experiments which made this thesis possible. As my best friends here, you never gave up on me and helped me develop the skills to be a successful young researcher. Last but not least, thank you for always believing in me and encouraging me especially when times were rough.

Contents

List of tables

List of figures

Chapter 1. Introduction

The main goal of tissue engineering in recent years is finding and developing novel and perfect materials for neo-organs, including synthetic biodegradable polymers and natural animal tissues [1]. With more and more research has been conducted in this field, decellularized tissues have attracted a lot of attention as an excellent alternative to make biological scaffolds [2-10]. A lot of different decellularized tissues have been studied, including small intestine submucosa (SIS), thoracic aorta, bladder, trachea and pericardium. In order to fabricate a tissue-engineered scaffold, there are three steps for them: extraction, decellularization and processing [11-15]. Compared with synthetic materials, the physical, chemical and biological properties of decellularized tissues are more similar to human tissues and therefore it might be easier for human cells to grow on them, which is very conducive to tissue remodeling and regeneration [16]. Meanwhile, there are a lot of growth factors, extra-cellular matrix (ECM), peptides and proteins in decellularized tissues, which is able to facilitate the vascularization. These features and advantages make decellularized tissues very suitable for regenerating both orthotopic and ectopic tissues [17]. For example, decellularized pericardium and SIS have already been applied for the tissue engineering of skin, bowel and bladder [16,17]. To improve the structural integrity and enhance the resistance against the enzymatic degradation, crosslinking with some chemicals is often opted [18]. Among all those different crosslinkers, “Genipin” is an attractive natural and biodegradable crosslinker because of its low cytotoxicity, anti-inflammatory, anti-oxidative and anti-thrombotic activities [19-23]. At the same time, the genipin crosslinked decellularized tissues can contribute to the proliferation and regeneration of human smooth muscle cells and

urothelial cells in vitro conditions and promote the angiogenesis without any pro-inflammatory responses, which is very exceptional for tissue-engineered scaffolds [22-26].

In general, we use decellularized tissues to regenerate the same type of tissues, but we used decellularized trachea to fabricate a neo-urinary conduit (NUC). For patients with invasive bladder cancer, their bladder is usually diseased and malfunctioning and has to be removed surgically. After the surgery, the patients need to use a conduit to pass urine out of their body or choose to have a new neobladder. In general, surgeons will use their gastrointestinal tracts to make a urinary diversion for patients although it might be detrimental for long-term health of patients with causing chronic kidney diseases and urinary tract infection [27-33]. However, to some extent, tissue-engineered urinary diversion, challenges associated with using GI tract [34-38]. Their application in pre-clinical phase has been proved to very successful [39]. However, when it comes to clinical phase, the results are not very satisfactory because tissue-engineered urinary diversion is not strong and biocompatible enough to function as an ideal neo-urinary conduit. In the first clinical phase, tissue-engineered urinary diversion supported the growth of human smooth muscle cells and human urothelial cells and regenerate cell layers as proven by histology testing. But it has a huge deficiency: it will form an abnormal amount of fibrous tissues in vitro and greatly contract and shrink over time without the ability to vascularize [36-39]. Based on the discovery mentioned above, we find that utilizing unseeded biological scaffold has great potential to regenerate urinary tissues in human body [40-42]. Also, the scaffold can be wrapped by the neighboring omentum, which it is likely to support formation of smooth muscle cells layers because it can offer excellent biological environment for cells [36,37,43].

Here, we explore the possibility of using decellularized rabbit trachea to act as a neo-urinary conduit (NUC) for patients with bladder cancer. By analyzing the inside structure of rabbit trachea, it is easy for us to find that there are some small cartilage rings in it, which can provide appropriate biomechanical characteristics for the scaffold [44-47]. In addition to sufficient mechanical strength, decellularized trachea exhibits the properties of an "ideal biological scaffold", namely biocompatibility, bioabsorbability, nonimmunogenity, support of cell attachment and growth, and an ability to induce angiogenesis [26]. We further crosslinked decellularized trachea with genipin. It is considered to be a naturally derived cross-linking agent and also known to improve the mechanical properties of decellularized tissues. The present study aimed to investigate the impact of the decellularization method and crosslinking agent on the compositional, structural, and mechanical integrity of rabbit tracheal extracellular matrix and to explore the biocompatibility of the decellularized trachea in pre-clinical phase.

Chapter 2. Materials and Methods

2.1 Decellularization process of rabbit tracheal matrices

The tracheas samples were decellularized using a previously described detergent-enzymatic treatment (DEM) [44,48-49]. First, the rabbit tracheae (Pel-Freez Biologicals, Arkansas) were washed three times with PBS for 30 minutes in total, and then snap frozen in the liquid nitrogen for 5 minutes and thawed at 37°C for 5 minutes, followed by detergent–enzyme decellularization. In the detergent step, the tracheas were incubated with 0.25% w/v sodium deoxycholate (Sigma) and 0.25% v/v Triton X-100 that are diluted in PBS and rotated continuously for 24 h at 37°C. Detergent was then removed and samples were washed in PBS for three times. In the enzyme step, DNase-I (150U/mL21; Sigma) and 50 mmol $MgCl_2$ (Sigma) diluted in PBS were used with continuous rotation for 24 h at 37°C. When the enzyme step was finished, the tracheae were washed with isopropanol for 24 h. And after washing three times (10 min at each) with PBS, the trachea samples were stored in PBS containing 1% antibiotic and antimycotic solution at 4 °C overnight, and the next cycle was initiated the following day.

2.2 Biomechanical tests

Both native and decellularized tracheae matrices were tested via the Bose tensile testing instrument (Enduratec ELF 3200, 225 N load cell) or the Instron tensile testing instrument (Load cell 5 N) to determine their strain characteristics. For this testing, the trachea specimens were first cut into small strips of 1.5 to 2.0 cm with width of approximately 5 mm from rabbit bladder (n=3). Then the samples were subjected to increasing uniaxial tensile testing until rupture, as confirmed by the loss of load and the appearance of tears in the tissue. The specimens were

clamped into sample holders, a pre-load (preliminary force) of 1 N was applied and the testing was initiated at a constant elongation rate of 0.1 mm/s at room temperature. The tensile tester recorded the stress and strain value in real time. Parameters such as tensile strength and linear elastic moduli values, along the longitudinal and circumferential (without the muscle tissues that joins the ends of the cartilage rings) axes of the sample strips were recorded and calculated using Microsoft Excel and Prism 6.0 software programs (Table 1).

An OMEGA DPG4000-1K digital manometer (OMEGA, Stamford, CT) was used to assess and record the compressive properties of each sample in real time. First, the specimen needed to be appropriately positioned in the instrument. One end of the sample was attached to a syringe pump (New Era Pump Systems, Farmingdale, NY), which was connected to the manometer by using a three-way adaptor, while the other end was fixed tightly. Then we used PBS to inflate the samples through a syringe pump at the rate of 0.2 mL/s until they were burst and mean burst pressure of the samples would be recorded.

Table 1. Comparative mechanical properties of decellularized tracheae.

Scaffold	Direction	UTS (MPa)	U Strain (%)	LEM (MPa)
Native	Longitudinal	0.62±0.09	40	0.29±0.07
	Circumferential	1.92±0.20	40	6.07±1.3
Decellularized	Longitudinal	0.34±0.07	55	0.06±0.02
	Circumferential	1.03±0.30	75	3.11±1.80
(Decellularized +cell-seeded)	Longitudinal	0.42±0.08	45	0.16±0.05
	Circumferential	0.80±0.13	40	1.2±0.20
(Decellularized +crosslinked +cell-seeded)	Longitudinal	0.55±0.10	35	0.35±0.05
	Circumferential	0.85±0.20	22	3.75±0.50
Control: rabbit bladder strips	randomly cut	0.20±0.06	330	0.05±0.01

UTS: Ultimate Tensile Strength

U Strain: Ultimate Tensile Strain

LEM: Linear Elastic Modulus

This table is reproduced with the permission from the publisher [70].

2.3 Scanning electron microscopy

To qualitatively evaluate the decellularized trachea matrix structure, tracheal (native and decellularized) matrices were fixed with 2.5% (v/v) glutaraldehyde(Aladdin, Shanghai, China) in the mixture of 100 mM sodium cacodylate buffer and 0.1% tannic acid (pH7.2-7.4) at 4°C. After rinsing in a 100 mM sodium cacodylate buffer containing 3% sucrose and 3.0 mM $MgCl_2$, the specimens were subjected to post-fixing in 0.8% potassium ferrocyanide and being reduced with 1% osmium tetroxide for one hour on ice in a dark room. After that, the samples were washed by distilled water, followed by ethanol gradient dehydration and hexamethyldisilanaze (HMDS) rinsing. When the tracheal specimen were completely dried in a desiccator, they were sputter coated with gold and observed by scanning electron microscopy (LEO 1530 FESEM).

2.4 Preparation of bioengineered scaffold and surface modification

In order to prepare bioengineered scaffold, the decellularized trachea specimen were cut into different smaller pieces in a cylindrical shape. The length of small scaffolds is around 7.5 mm. We used PBS mixed with 4% ethanol and 0.2% peracetic acid (PAA) to sterilize the scaffolds. The whole sterilizing process should last for 6 h. When the sterilization step was completed, we continued to wash the tracheal scaffolds with PBS five times, then with isopropanol and kept it in isopropanol solution for 24 h. Finally, we wash the scaffolds three times in PBS solution. In order to make sure various cells can be attached to the bioengineered scaffold, we tried several different ways to modify the surface of the scaffold. *Genipin cross-linking treatment*: The decellularized tracheae were cross-linked in 1% w/v aqueous genipin (Merlin, Hangkong, China) solution buffered with PBS and ethanol mixture (70/30) for 4h at 37 °C under constant agitation.

After the crosslinking, the color of the decellularized tracheae would become light blue. The treated tissues were then thoroughly washed with sterile PBS and peracetic acid, with each washing cycle lasting for 10 min. Finally, the light blue color would disappear. *Collagen-I coating*: we kept our tracheal scaffold in collagen-I solution (5 mg/mL in HCl, CosmoBio) and then used a piece of tissue paper to absorb the extra collagen-I solution. After that, the scaffold was submerged in a neutralizing solution for 5 min, which is made up of 8.8 mL of Dulbecco's Modified Eagle's Medium (DMEM) with 1 g/L D-Glucose, L-glutamate, 110 mg/L Sodium Pyruvate (Life Technologies, NY), 0.2 mL of HEPES (x1, 1M) and 1.0 mL of fetal bovine serum (FBS) [50]. Finally, the scaffold was vitrified in a controlled humidity chamber for 4h at 40% RH and 39°C [50-51]. *Oxygen-plasma treatment*: we put the tracheal scaffold in plasma with a pressure of 280-290 mmHg at room temperature for 10 min. The oxygen in the atmosphere could help activate free radicals in the surface of the scaffold. After keeping the scaffold in 10 mL solution containing 10 % (v/v) polyacrylic acid (PAA) and 0.5 mM $NaIO_3$, we exposed it to UV (36 mW/cm^2, DYMAX Light Curing Systems 5000 Flood, Torrington, CT) for 2 min to initiate the photo-polymerization of PAA to modify the surface of the scaffold. *RGD (a cell-integrin binding peptide with sequence-Arginine-Glycine-Aspartic acid) treatment*: we soaked the scaffold in NHS-PEG-MAL solution (3.4 kDa, JenKem) at a concentration of 1 mg/mL and put them in a shaker for half an hour. Then we transferred the scaffold to the RGD solution (1 mg/mL, Biomatik), put them in a shaker for 2h and finally wash with PBS for one time.

2.5 Establishment of Smooth Muscle and Urothelial cell lines

We purchased both human smooth muscle cells (hSMCs) and urothelial cells (hUCs) from the ScienCell Research Laboratories (Carlsbad, CA). Human smooth muscle cells were grown in

Dulbecco's modified Eagle's medium (DMEM) and Ham's F-12 nutrient mixture (3:1) (Sigma), containing L-Glutamine, 15 mM HEPES and 1.0 ng/ml basic FGF (Life Technologies, Grand Island, NY) supplemented with 10% fetal bovine serum (FBS) and 1% Penicillin/Streptomycin.

We started counting passage number when we were first able to pass the cells into 35-mm plates (passage 1). The hSMCs were harvested at passage 3. Urothelial cells were seeded in a growth media consisting of basal UC medium (Sciencell, CA) and UC growth factor supplemented with 1% Penicillin/Streptomycin (Life Technologies). The hUCs were harvested at passage 4. Two to three days later, both hSMCs and hUCs needed to be transferred into new wells. All the cells must be cultured in in a humid environment at 37°C and 5% CO_2.

2.6 Growth of hSMCs and hUCs in the surface of tracheal scaffold

We disaggregated the hSMCs at passage 4 using trypsin (0.25%, 5 mL per tissue culture plate) and centrifuged them at 1,000 rpm for 5 min. Then we seeded the detached cells in hSMCs growth medium to increase the cell density to approximately 2 million cells/ml. After that, we transferred the bioengineered scaffold and hSMCs growth media to a cryotube (Nunc, 3.6 mL), and then put it inside a centrifuge tube (15 mL, Becton Dickinson), followed by shaking for 6h at 37°C until the cell density reached 2 million cells per scaffold (length of 0.75 cm). Finally, we took the scaffold out and put in non-tissue culture well plates to keep growing hSMCs for one week. After seven days, we transferred the tracheal scaffold seeded with hSMCs to small cut pipette tips (1 mL, ThermoFisher). One end of the small cut pipette tips was sealed by parafilm, while on the other end, we tried to grow hUCs at passage 4 on the inner lumen of the tracheal scaffold. Then the small cut pipette tips were kept in cryotubes, which had already been put inside centrifuge tubes previously. They had to be shaken continuously for 4h at 37°C. After 4h,

we took out the scaffold and kept it in 12 well-tissue culture plates filled with both hSMCs growth medium and hUCs growth medium (50/50). All the cells must be cultured in in a humid environment at 37°C and 5% CO_2. For the study of cell morphology, cells should be cultured in shorter time and the bioengineered scaffold needed to be cut into several small rings (3 mm x 3 mm). The scaffold could be cultured with either hSMCs (75,000 cells per scaffold) or hUCs (12,500 cells per scaffold) or both hSMCs and hUCs in appropriate cell growth media, respectively.

2.7 Immunostaining

Immunostaining consists of two parts: immunofluorescence staining (IF) and immunohistochemistry (IHC) [52]. For immunofluorescence staining, we cut the trachea samples embedded in paraffin into smaller sections at a 5 μm thickness with a Cryo-mill (Leica), then submerged them in a 40°C water bath for some time and finally put all the samples into glass microscope slides. These glass microscope slides had to be left at 40°C overnight. In order to get rid of paraffin and hydrate the samples, we first washed the sections with xylene and then graded alcohol (100%, 95%, 80%) and eventually with distilled water. Pretreatment of sections with microwave heating for 45 minutes in a target retrieval solution (Dako, CA) was used for antigen retrieval. After heating, sections must be cooled until room temperature for further steps. These sections were covered with serum-free protein blocking buffer (Dako code X0909) to reduce nonspecific staining for 1h at 37°C in a dark chamber and then immunostained overnight at 4°C with primary antibody (alpha-smooth muscle actin and pan cytokeratin, Abcam). After washing with a Dako wash buffer for 5 min, the sections were incubated with secondary antibodies and then covered with a 1:800 dilution of streptavidin peroxidase complex at room temperature for

2h, followed by the same Dako wash buffer rinsing for 5 min. When we finished the incubation of secondary antibodies, all the sections were washed in distilled water, dehydrated in graded alcohol (80%, 95%, 100%) and xylene, and mounted with a Permount mounting solution on a cover slip. Sections were also stained with 40-6-diamidino-2-phenylindole (DAPI; KeyGEN, Nanjing, China) to detect nuclear material. All stained sections were evaluated by 2 pathologists independently and graded as score 1-negative to few cells positive (less than 5% cells), score 2-heterogeneously positive (range 5% to 80%) and score 3-uniformly positive (greater than 80%), as reported previously [53].

For immunohistochemistry, trachea samples (native and decellularized) were fixed for 24 h in 10% neutral buffered formalin solution in PBS (pH 7.4) at room temperature. After fixation, the samples were rinsed in distilled water, dehydrated in graded alcohol, embedded in paraffin, and sectioned at 6 μm thickness. In order to remove paraffin, rehydrate the samples and retrieve antigen, we soaked the samples in in Trilogy (Cell Marque, AR) in a pressure cooker at 126ºC under the pressure of 23 psi. Then we blocked endogenous Peroxidase and Alkaline Phosphatase using a Dual Endogenous Block (DAKO North America Inc., CA). Sections were incubated at 4ºC for 45 min with rabbit primary antibodies (cleaved caspase 3, Cell Signaling Technology, MA; vimentin, Cell Signaling Technology, MA; Ki67, Abcam, MA; alpha-smooth muscle actin, Abcam, MA). After washing, PowerVision Poly-HRP anti-Rabbit IgG (Leica Biosystems, IL) as secondary antibody was applied for 30 min. We detected the antibody complex with diaminobenzidine (DAB), which is the color substrate of horseradish peroxidase (HRP). Eventually, these sections were counterstained with hematoxylin (Richard-Allen Scientific,

Kalamazoo, MI), mounted and then examined under Zeiss Discovery V2 dissection imaging microscope.

2.8 Gene expression by quantitative real-time polymerase chain reaction

In this part, we examine the gene expression of different cells by using a quantitative real-time polymerase chain reaction (qRT-PCR) [52]. For sample preparation, we collected the fresh samples at various time points. After that, all the biological specimen were instantly shock-frozen in liquid nitrogen and stored at -80°C until further use. For RNA extraction and complimentary cDNA synthesis, we thawed the frozen samples and adapted the protocol from RNeasy mini kit (Qiagen, CA) to permit the isolation of total RNA from those specimens. After RNA extraction, the total RNA (300 ng) was then transcribed to cDNA by using random hexamers and Ready-To-Go You-Prime First-Strand Beads (GE healthcare, PA) serving as primers in a total volume of 20 μL. We put the mixed solution in a 96 well plate and ran the PCR reaction in triplicates. mRNA encoding for β-actin or glyceraldehyde 3-phosphate dehydrogenase (*GAPDH*) was processed as used as a housekeeping gene. Its product served as the control for RNA and relative quantification. For the real-time quantitative RT-PCR, it is carried out on an Applied BioSystems 7900HT thermocycler (Applied Biosystems, Inc.) using the following conditions: 50 °C for 2 min and 95 °C for 10 min, followed by 40 cycles of 95 °C for 15 s and 60 °C for 1 min. Raw data can then be analyzed with SDS Relative Quantification Software version 2.2.3 (Applied BioSystems, Inc.), generally using the automatic cycle threshold (Ct) setting for assigning baseline and threshold for Ct determination. Finally, we used the probe TaqMan^{R} Universal Mix II, No UNG (Thermofisher, MA) to detect the expression of following genes (Table 2): Smooth-muscle alpha-actin (*ACTA2*), Transgelin (*TAGLN*), smooth muscle

myosin heavy chain (*MYH11*), smooth muscle basic (h1) calponin (*CNN*), Myocardin (*MYOCD*), smoothelin (*SMTN*), non-muscle myosin heavy chain B (*MYH10*), cellular-retinol binding protein-1 (*RBP1)* vimentin (*VIM)*, collagen-I alpha1 (*COL1*), collagen-III alpha1 (*COL3*), elastin (*ELN*), laminin (*LAMA1)*, cytokeratin 5 (*KRT 5)*, cytokeratin 18 (*KRT18*), uroplakin 3 (*UPK3A*), caspase 3 (*CASP3*) and S100 calcium-binding protein A4 (*S100A4*).

Table 2. Taqman assays used for *q*PCR studies.

Target gene	Taqman assay ID	Reference ID*	Exon boundary	Assay location	Amplicon length
ACTB	Hs01060665_g1	NM_001101.3	2-3	208	63
CNN1	Hs00154543_m1	NM_001299.4	1-2	229	93
MYOCD	Hs00538071_m1	NM_001146312.1	7-8	1015	63
COL1A1	Hs00164004_m1	NM_000088.3	1-2	230	66
COL3A1	Hs00943809_m1	NM_000090.3	48-49	3940	65
SMTN	Hs00199489_m1	NM_001207017.1	14-15	2176	52
ELN	Hs00355783_m1	NM_001278918.1	1-2	484	71
RBP1	Hs010111512_g1	NM_001130992.1	1-2	371	77
TAGLN	Hs01038777_g1	NM_001001522.1	2-3	700	65
MYH11	Hs00975796_m1	NM_001040113.1	38-39	5422	53
VIM	Hs00958111_m1	NM_003380.3	3-4	1030	65
ACTA2	Hs00426835_g1	NM_001141945.2	2-3	613	105
MYH10	Hs00992055_m1	NM_001256012.1	29-30	381	83
CASP3	Hs00234387_m1	NM_004346.3	4-5	441	100
S100A4	Hs01569256_m1	NM_019554.2	2-3	93	59
LAMA1	Hs00300550_m1	NM_005559.3	1-2	158	77
KRT5	Hs00361185_m1	NM_000424.3	7-8	1601	133
KRT18	Hs02827483_g1	NM_000224.2	1-2	531	64
UPK3A	Hs00199590_m1	NM_001167574.1	3-4	372	58

*Reference ID sequences represent cDNAs.

This table is reproduced with the permission from the publisher [70].

2.9 Statistical analysis

All quantitative data are expressed as the mean ± standard deviation of three separate experiments. Statistical analysis was performed by unpaired t-test with Welch's correction for post-hoc comparisons. Differences were considered significant at the 95% level ($p < 0.05$). Statistical significant values with $p < 0.05$ were marked as **.

Chapter 3. Results

3.1 Characterization of decellularized rabbit tracheal matrix

The decellularized trachea retained the typical gross anatomical structure of native trachea, compared to freshly harvested tissues (Figure 1A and 1B). After decellularization, the three-dimensional architecture and composition of the tracheal matrix remained intact and were virtually unaltered, including the preservation of the lumen, middle cartilage and outer layers. And quantitative analysis of histologic sections revealed that DNA concentration in the tissue was substantially decreased from 1716±76 ng/mg in native trachea to 163±54 ng/mg after decellularization (Fig. 1C). Nuclei stained with hematoxylin and eosin (H&E) were almost completely removed in the noncartilaginous tissue, and only a small number of nuclei remained in the thick cartilage (Fig. 1D and 1E). Safranin-O staining showed that glycosaminoglycan (GAG) expression was mainly concentrated to the cartilaginous region. After decellularization, there was a significant loss of glycosaminoglycan in the outer layer of the tracheal cartilage (Fig. 1F and 1G). Masson's trichrome staining (Fig. 1H and 1I) showed that only the connective tissues (blue) and some cell nuclei (dark red) could be stained in the decellularized scaffold, while cytoplasm (pink) can be stained in native trachea.

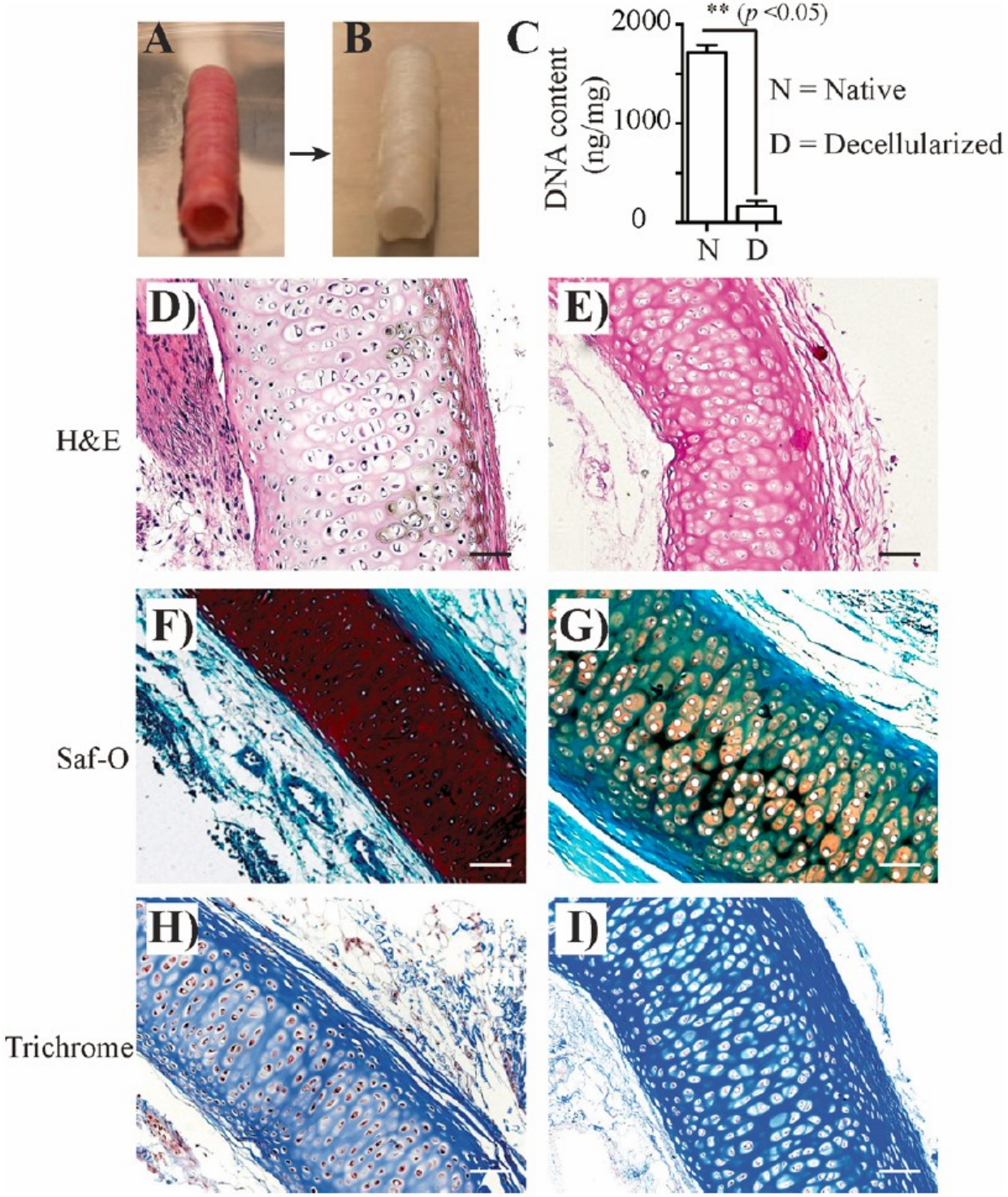

Figure 1. Characterization of decellularized rabbit tracheal matrix. The native trachea **(A)**, after detergent-enzymatic treatment **(B)**. DNA content **(C)**, hematoxylin and eosin (H&E)

staining **(D&E)**, Safranin-O staining **(F&G)** and Masson's trichrome staining **(H&I)** of the tracheal scaffold before and after decellularization. (** denotes statistical significant values with $p < 0.05$) This figure is reproduced with the permission from the publisher [70].

3.2 Viscoelastic properties of the bioengineered tracheal scaffold

Uniaxial tensile tests were carried out on the decellularized tracheal matrices, showing that the bioengineered scaffold can be a good option for constructing a neo-urinary conduit (NUC) with a combination of perfect flexibility and tensile strength. The tensile tests were performed in both longitudinal and circumferential direction and the related results were characterized by slope-changing J-curves (Fig. 2A, 2B). The ultimate tensile strength (UTS) was the maximum stress at the reversal point of the engineering stress–strain curve and the initial linear elastic modulus (LEM) was measured within the linear region of initial 0% to 10% strain. In Table 1, we find in longitudinal direction, both UTS and LEM values significantly decreased in the decellularized trachea compared with the native tracheal matrices (UTS: native *vs* decellularized scaffolds: 0.62±0.09 MPa *vs* 0.34±0.07 MPa; LEM: native *vs* decellularized scaffolds: 0.29±0.07 MPa *vs* 0.06±0.02 MPa). In circumferential direction, there was a similar decrease in UTS and LEM (UTS: native *vs* decellularized scaffolds: 1.92±0.20 MPa *vs* 1.03±0.30 MPa; LEM: native *vs* decellularized scaffolds: 6.07±1.30 MPa *vs* 3.11±1.80 MPa). For the UTS of genipin- crosslinked samples, there was an increase in longitudinal direction (from 0.34±0.07 MPa to 0.55±0.10 MPa), but a slight decrease in circumferential direction (from 1.03±0.30 MPa to 0.85±0.20 MPa). And for LEM values, there was an increase in both two directions (longitudinal direction: from 0.06±0.02 MPa to 0.35±0.05 MPa; circumferential direction: from 3.11±1.80 MPa to 3.75±0.50

MPa). We also used rabbit bladder strips as a control (Fig. 2H) with the UTS of 0.20±0.06 MPa, LEM of 0.05±0.01 MPa and ultimate tensile strain of 330%.

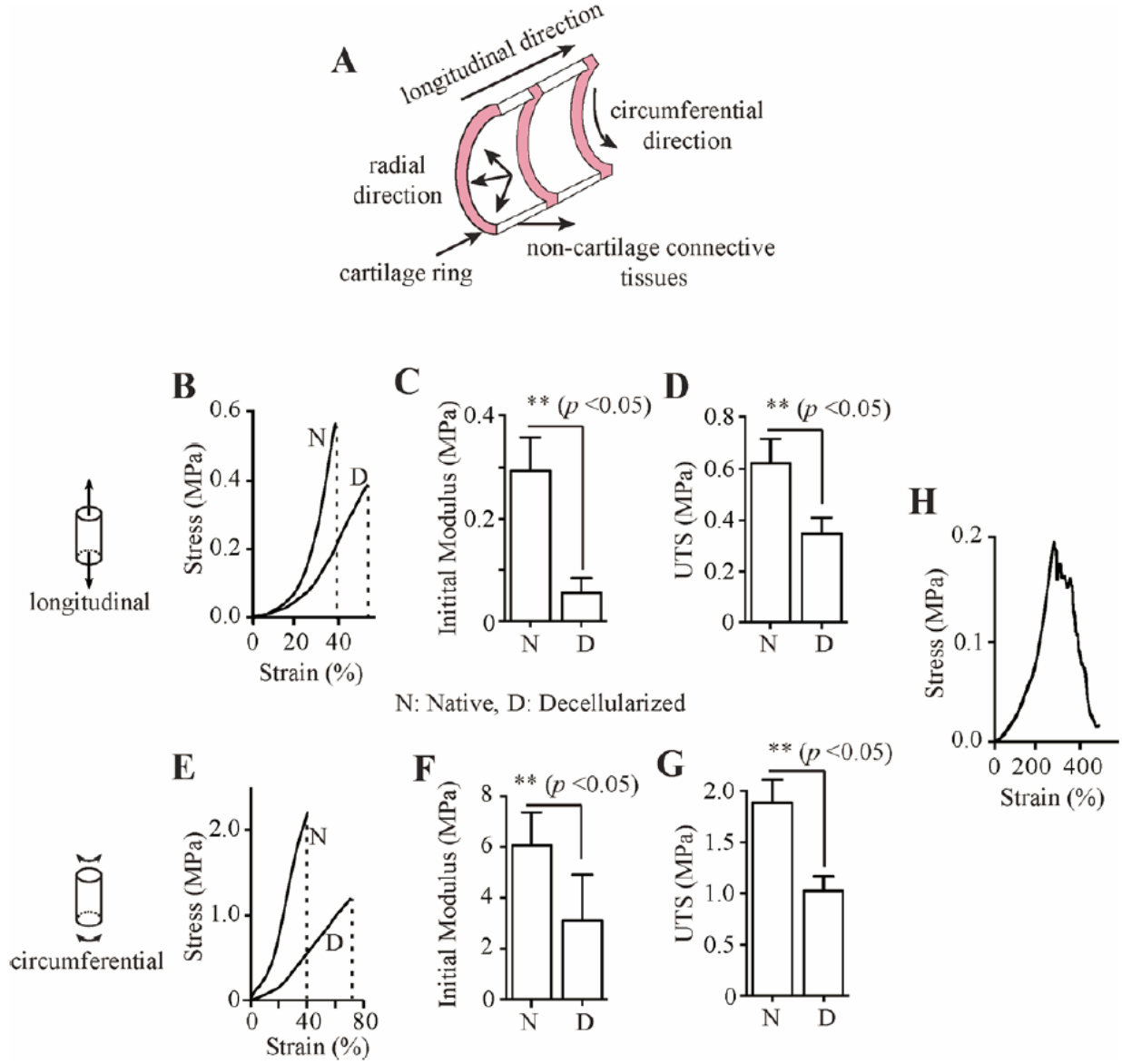

Figure 2. Mechanical characteristics of native vs. bioengineered tracheal scaffolds. The tensile tests were performed in both longitudinal and circumferential direction **(A).** Stress-strain curves **(B)**, initial linear elastic modulus (LEM) **(C)**, the ultimate tensile strength (UTS) **(D)** of the native and decellularized scaffolds in longitudinal direction. Similarly, we got the stress-

strain curves **(E)**, LEM **(F)** and UTS **(G)** results in circumferential direction. We also used a rabbit bladder as control and got its stress-strain curve **(H)**. This figure is reproduced with the permission from the publisher [70].

3.3 Cell attachment on surface-modified decellularized trachea

In order to improve the cell adhesion on the decellularized scaffold, we tried several different ways to modify the surface of the scaffold: oxygen-plasma treatment, collagen-I coating and RGD (a cell-integrin binding peptide with sequence-Arginine-Glycine-Aspartic acid) treatment (Fig. 3A-D). For RGD treatment and collagen-I coating, human smooth muscle cells (hSMCs) were able to grow on the modified surface of the scaffold and the decellularized tracheal maintained a sufficient extracellular matrix and structural rigidity. For oxygen-plasma treatment, it caused some changes in the structure of the decellularized scaffold. However, these modified surfaces cannot provide the scaffold with a consistent and sufficient cell adhesion, so we had to get rid of hydrophobic or lipid components from native trachea in the process of decellularization to enhance cell attachment.

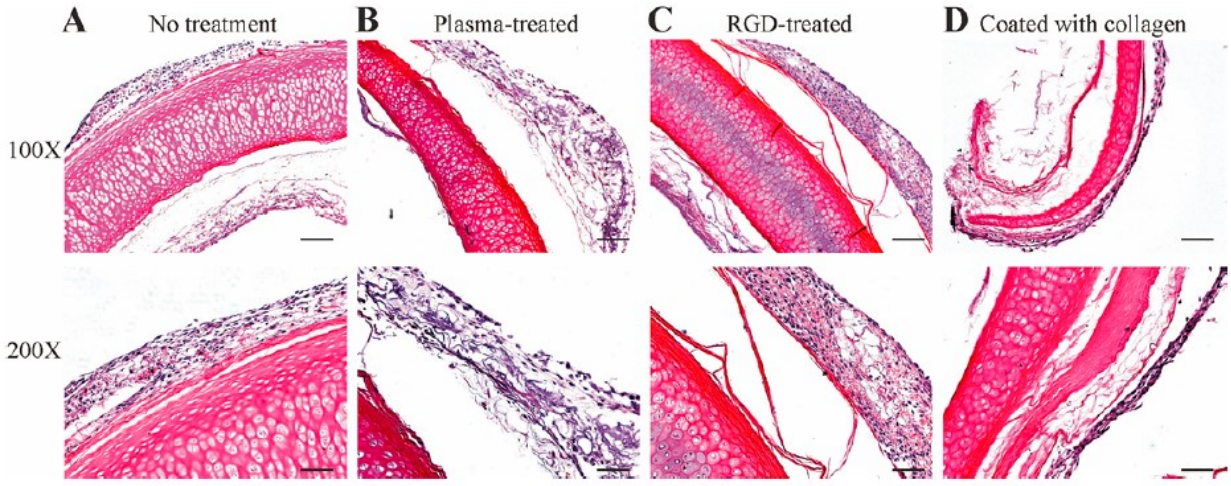

Figure 3. Decellularized tracheal scaffold with modified surfaces. In order to improve cell

attachment of the decellularized scaffold **(A)**, we tried several different ways to modify the surface of the scaffold: oxygen-plasma treatment **(B)**, RGD (a cell-integrin binding peptide with sequence-Arginine-Glycine-Aspartic acid) treatment **(C)** and collagen-I coating **(D)**. (scale bar = 200 μm for 100X, and = 100 μm for 200X) This figure is reproduced with the permission from the publisher [70].

3.4 Morphological study of human urothelial cells and smooth muscle cells on the scaffolds

Cell morphologies on the decellularized tracheal scaffolds in different condition were examined by scanning electron microscopy (SEM). For the trachea without crosslinking, there is a clear boundary between the luminal and outer surfaces (Fig. 4A). And the lumen has a lot of smaller and finer fibers and thereby exhibits a smooth surface, while the outer surface possesses thicker and bigger fibers and shows a much rougher surface. For the genipin-crosslinked trachea, we can observe the same morphologies, but they are more apparent and obvious. When we grow the human urothelial cells (hUCs) on the decellularized tracheal scaffold, hUCs are able to grow in the lumen, outer surface, edge and cartilage rings of the trachea (Fig. 4B). In the lumen, the urothelial cells are tightly arranged and form a uniform pattern (denoted by arrow marks). In the outer surface, the cells are more separate and in a spherical shape, which means they are not proliferating well. At the edges, there is a distinct boundary between lumen and the outer surface so that we can observe the cell morphologies of both two areas more clearly. In the cartilage ring, the cells are surprisingly growing and spreading better than muscle regions. Also, for the crosslinked trachea seeded with the hUCs, there is not a huge difference in the cell morphologies of lumen, outer surface, edge and cartilage ring.

For the decellularized trachea scaffold seeded with human smooth muscle cells (hSMCs), hSMCs are growing in the shape of an elongated spindle and adopt a very similar arranging pattern in the lumen, outer surface and edges of the scaffold (Fig. 4C). For the genipin-crosslinked one, hSMCs are proliferating better and organizing themselves more densely on all the three surfaces.

For the decellularized trachea scaffold seeded with both hSMCs and hUCs in a mixed cell culture medium (hSMCs growth medium/ hUCs growth medium: 50/50), the morphological behavior of hSMCs and hUCs is a little similar ((Fig. 4D). For hSMCs, they are spreading and growing overwhelmingly in the lumen, outer surface, edge and cartilage rings of the tracheal scaffold. But compared with hSMCs cultured in only hSMCs growth medium, they are in a shorter-spindle shape and appear to have more protrusions. For hUCs, they are able to grow and proliferate in the lumen, edge and cartilage rings of the tracheal scaffold, but unable to spread and grow on the outer surface. Under the mixed cell culture condition, hUCs are round and compact and show tight cell-to-cell contacts, which is similar to those grown in only hUCs growth medium. And for the genipin-crosslinked trachea seeded with both hUCs and hSMCs, we do not observe many different cell morphologies in the lumen, outer surface, edge and cartilage rings of the scaffold.

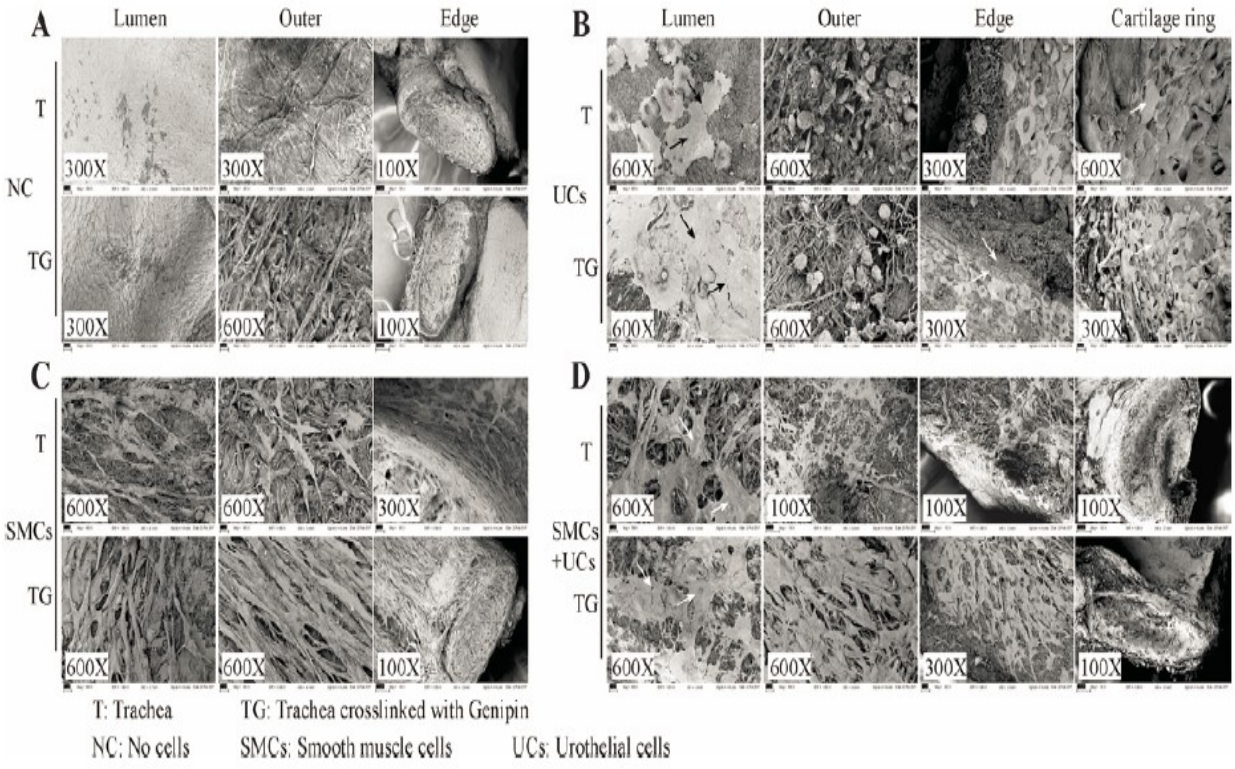

Figure 4. Morphologies of human urothelial cells and smooth muscle cells on the decellularized and genipin-crosslinked scaffolds. The fiber morphologies of lumen, outer surface and edge in the decellularized tracheal scaffold (control without crosslinking) (T) and in the genipin-crosslinked scaffold (TG) were examined by SEM **(A)**. After we seed the decellularized tracheal scaffold with human urothelial cells (hUCs), hUCs are able to grow in the lumen and cartilage rings of the trachea, but prefer the luminal surface with uniform and tight cell arrangement for both T and TG **(B)**. In contrast, hSMCs can spread and proliferate in all the surfaces of the decellularized scaffold with the shape of an elongated spindle. Genipin-crosslinking seems to promote the growth of hSMCs **(C)**. For the decellularized trachea scaffold seeded with both hSMCs and hUCs in a mixed cell culture condition, hSMCs are spreading and growing overwhelmingly in the lumen, outer surface, edge and cartilage rings of the scaffold, while hUCs still prefer growing in the lumen **(D)**. (scale bar = 100 μm for 100X, 200 μm for

300X and 10 μm for 600X) This figure is reproduced with the permission from the publisher [70].

3.5 Biomechanical properties of the cell-seeded decellularized trachea

In order to know whether the cell culture on the surface of the scaffold would influence its biomechanical properties, we compare the uniaxial tensile testing results of the cell-seeded decellularized trachea with that of the decellularized trachea. According to Fig. 5A and Table 1, we discovered that in longitudinal direction, there was a slight increase in UTS values after cell seeding (from 0.34±0.07 MPa to 0.42±0.08 MPa), but a decrease in ultimate tensile strain (from 55% to 45%). And in circumferential direction, there was a decline in the values of both UTS and ultimate tensile strain after the growth of various cells (UTS: from 1.03±0.30 MPa to 0.80±0.13 MPa; ultimate tensile strain: from 75% to 40%).

3.6 Immunostaining

For immunofluorescence staining, pan-cytokeratin is a cytoskeleton marker for human urothelial cells (hUCs), while alpha-smooth muscle actin is a special marker for human smooth muscle cells (hSMCs). With the use of 40-6-diamidino-2-phenylindole (DAPI; KeyGEN, Nanjing, China), we can detect the nuclei in various cells, which is blue in Fig. 5B. Also, for the tracheal scaffolds grown with both hSMCs and hUCs for only three days, we can easily find out the existence of pan-cytokeratin (red) in Fig. 5B, while there is no red for the scaffolds seeded with both cells for a week. And for hSMCs, we can find out the positive staining for alpha-smooth muscle actin (green) in both three days and one-week cell-cultured scaffolds.

For immunohistochemistry, alpha-smooth muscle actin (SMA) is a contractile phenotype marker for hSMCs, while vimentin is a synthetic phenotype marker for hSMCs; Ki67 is a cellular marker for proliferation; cleaved caspase 3 is a marker related to cellular apoptosis. In Fig. 5C, we can discover the existence of SMA and vimentin in some vessel-like structures (marked in dotted circles). Meanwhile, we also observe the positive staining of Ki67 and cleaved caspase 3, which means some cells are undergoing proliferation and apoptosis, respectively.

3.7 Gene expression

For the genipin-crosslinked scaffold seeded with both human smooth muscle cells (hSMCs) and human urothelial cells (hUCs), the level of gene expressions for different cells were evaluated by quantitative real-time polymerase chain reaction (RT-qPCR). According to Fig. 5D, we observed that the gene expression level of *ACTA-2* (2 folds), *TAGLN or SM 22-alpha* (8 folds), *CNN1* (6 folds), *MYOCD* (1.7 folds), *MYH10* (3 folds), *RBP1* (2.3 folds), *VIM* (2.5 folds), *ELN* (9 folds) and *CASP3* (2 folds) were upregulated significantly, while *MYH11*, *SMTN*, *COL 3* were only increased slightly. For *COL 1* and *S100A4*, although there was a decrease at the beginning stage, their gene expression levels were ultimately increased in week four. Besides that, *LAMA1* (11 folds) and *KRT 5* (12 folds) were downregulated, while *UPK3A* was not detected through one week to four weeks. Furthermore, the genes with increased values of expression are the markers of hSMCs, which confirmed the existence of smooth muscle cells, while the undetected gene and the genes with decreased values of expression are the markers of hUCs, which means the disappearance of urothelial cells.

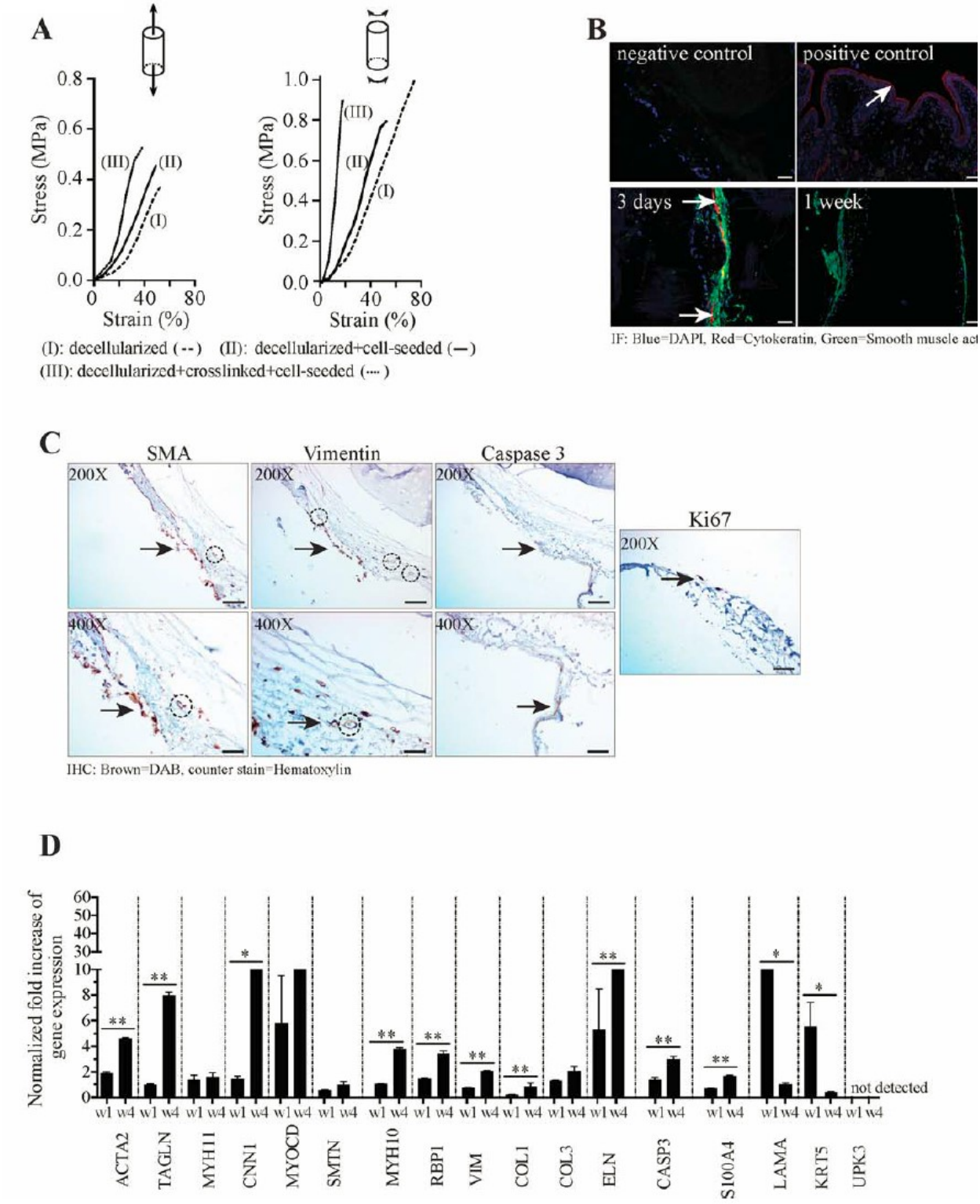

Figure 5. Immunostaining and gene expression for both hSMCs and hUCs. The stress-strain curves reveal that cell seeding and genipin-crosslinking can help improve the mechanical

properties of the decellularized tracheal scaffold **(A)**. We performed the immunofluorescence staining (IF) for the decellularized tracheal scaffold seeded with cells for three days and one week and pan-cytokeratin (red), alpha-smooth muscle actin (green) and nuclei (blue) were stained **(B)**. We also did immunohistochemistry (IHC) for the tracheal scaffold and found out the presence of hSMCs markers for both contractile and synthetic phenotype (SMA and vimentin). We also observe the proliferation (Ki67) and apoptosis (cleaved caspase 3) of various cells **(C)**. The results of gene expression showed that the genetic markers for hSMCs were upregulated over time, while the genetic markers for hUCs were downregulated or not detected **(D)**. Cleaved caspase 3 and S100A4 are the hSMCs markers for apoptosis and fibrosis, respectively. LAMA, KRT5 and UPK3 are the genetic markers of hUCs and UPK3 is only present on the layer of stratified urothelium. This figure is reproduced with the permission from the publisher [70].

Chapter 4. Discussion

Tissue engineering provides a promising approach for constructing a neo-urinary conduit (NUC). The selection of the most reasonable bioengineered scaffold is highly important for a suitable engineering process and subsequent in situ organ function. As an ideal scaffold, it should mimic the target tissue environment and maintain the required tissue-specific mechanical properties. Various natural and synthetic materials have been applied to trachea tissue engineering, including poly(glycol acid), poly(lactic acid), collagen, hyaluronic-acid, and chitosan [54-57]. Although good mechanical stability and cell growth have been obtained in some cases, these constructs are far from translation into clinical applications because their functionality, biomechanics, viability, and adequate and continuous vascularization remain undetermined. However, decellularized tissue currently appears to be the most promising approach to obtaining suitable scaffolds to engineer a variety of tissues and organs, not only because they have a mechanic function but also because they can affect cell proliferation, migration, differentiation and, as a consequence, tissue regeneration and remodeling. Various detergents and solutions and physical techniques have been used to obtain such a scaffold [58]. Most of them have been found to be highly efficient at removing cellular materials but also caused disruption of glycosaminglycan (GAG) and substantially reduced laminin and fibronectin ECM content, thereby compromising the ability of the scaffolds to provide mechanical support during the remodeling process [59]. In this paper, we used a detergent enzymatic approach (DEM) based on the use of deoxycholate and DNase, which is the only clinically acceptable method for producing a decellularized trachea. Using DEM, the three-dimensional architecture and composition of the tracheal matrix remained intact and was virtually unaltered, including the preservation of the

lumen, middle cartilage and outer layers. In Fig. 1D and Fig. 1E, the nuclei were effectively dissolved by DNase and removed from the luminal and outer layers. The DEM, however, has different effects on non-cartilaginous tissues and cartilage. It is highly efficient at removing cells from the non-cartilaginous tissues, but not from cartilage and that is the reason why there are a small number of nuclei remained in the deep cartilage. In addition, the decellularization process will affect the composition and structure of the extracellular matrix. Glycosaminoglycan (GAG) is the main substance of the native tracheal cartilage, and it is able to provide the trachea with sufficient mechanical strength to resist compressive forces. In Fig. 1F and Fig. 1G, we observed a loss of glycosaminoglycan content in tracheal cartilage, which is confirmed by the decrease of a dark red-brownish staining in the pictures [44,58-60].

Uniaxial tensile tests were carried out on the decellularized tracheal matrices, so that we can know whether the decellularization process will affect the biomechanical properties of the bioengineered scaffold ((Fig. 2A-H & Table 1). The tensile tests were performed in both longitudinal and circumferential direction and the related results could be characterized by slope-changing J-curves due to the structural and compositional anisotropy of various biological tissues. For rabbit trachea, it is composed of stiff cartilage rings and compliant soft muscle regions, which is responsible for the anisotropy of trachea. For the pull in longitudinal direction, the muscle tissues will first be stretched and then the cartilage rings will start to take part in the tensile testing and be pulled afterwards. In the stress-strain curves of both native and decellularized tracheal scaffolds: from 0 to 20% (strain coordinate), the slope of the J-curve is very small, which means the scaffold can be easily pulled and elongated because of the only participation of muscle tissues; from 20% to 80%, the slope of the J-curve is very high,

suggesting that the scaffold is able to withstand more applied forces due to the participation of both muscle tissues and cartilage rings. For the pull in circumferential direction, both muscle tissues and cartilage ring will take part in the tensile testing and resist the applied force at the very beginning. This can explain the fact that the ultimate tensile strength (UTS) and linear elastic modulus (LEM) values of both native and decellularized scaffolds in in circumferential direction are higher than those in longitudinal direction.

In addition, we observe that in longitudinal direction, there is a significant decrease in values of LEM and UTS after the DEM decellularization process, while there is an increase for the value of ultimate tensile strain (UTS: native *vs* decellularized scaffolds: 0.62±0.09 MPa *vs* 0.34±0.07 MPa; LEM: native *vs* decellularized scaffolds: 0.29±0.07 MPa *vs* 0.06±0.02 MPa; ultimate tensile strain: native *vs* decellularized scaffolds: 40% *vs* 55%). And the increase of the strain values of the decellularized scaffold represents the increase of compliance (change in dimension per unit stress) of the scaffold. In circumferential direction, there is a similar decrease in UTS and LEM, while an increase in the value of ultimate tensile strain after decellularization (UTS: native *vs* decellularized scaffolds: 1.92±0.20 MPa *vs* 1.03±0.30 MPa; LEM: native *vs* decellularized scaffolds: 6.07±1.30 MPa *vs* 3.11±1.80 MPa; ultimate tensile strain: native *vs* decellularized scaffolds: 40% *vs* 75%). The change of the values of LEM, UTS and ultimate tensile strain can be attributed to the loss of cellular elements and glycosaminoglycan (GAG) [26,36]. When we increase the volume compliance (change in storage volume capacity to initial storage volume capacity) of the decellularized scaffold to three times, we discover it can maintain the complete matrix structure under the radial burst pressure of 155 Hg. But if we increase the value of pressure, it will burst and start leaking water from inside.

In order to improve the stability and mechanical response of tissue-engineered tracheal scaffolds, we tried to crosslink the decellularized tracheal scaffold with genipin. Genipin is completely naturally derived (it is obtained from geniposide, isolated from the fruits of gardeniajasminoides) and can react spontaneously with amino acids or proteins, inducing an intramolecular and intermolecular cross-linking cyclic structure within collagen fibers. For tissue-engineering, genipin has been shown to be effective in improving the stability of collagen-based biomaterials, forming stable cross-linked products with less *in vitro* cytotoxicity and a lower *in vivo* inflammatory response [19-25,61]. Also, it has been proved that the genipin-crosslinked decellularized scaffold can persist *in vivo* without being subjected to host enzymatic degradation [62,63]. However, for a harsher urine-containing environment, there are still a lot of details that need to be investigated.

In summary, the uniaxial tensile testing results reveal that there was a reduction in the mechanical performance for the tracheal scaffold after decellularization compared to native tracheal matrices, which can be explained by a significant loss of glycosaminoglycan content in tracheal cartilage during the decellularization process (Fig. 2B-G). For the cell-seeded scaffold, hSMCs spread and proliferated on the outer surface of the scaffold and were not able to penetrate into the cartilage ring.

In order to make different cells able to adhere to the decellularized tracheal scaffold, we tried several different methods to modify the surface of the scaffold: oxygen-plasma treatment, collagen-I coating and RGD (a cell-integrin binding peptide with sequence-Arginine-Glycine-Aspartic acid) treatment. For RGD treatment and collagen-I coating, the modified surfaces of the decellularized tracheal scaffolds were able to allow the attachment and proliferation of human

smooth muscle cells (hSMCs), without altering the internal structure of the matrix. For oxygen-plasma treatment, it became much stiffer than normal decellularized tracheal scaffolds, which was because of the possible internal crosslinking of some functional moieties in the tracheal scaffold. However, the abovementioned methods failed to provide the decellularized scaffold with a consistent and sufficient cell adhesion, so we chose to get rid of hydrophobic or lipid components in the process of decellularization, which are likely to influence the attachment and growth of smooth muscle cells [64]. Herein, we tried to wash the decellularized tracheal scaffold with isopropanol [65], so that we could remove any visible hydrophobic or lipid components from the decellularized trachea and finally achieved perfect and sufficient consistency in cell attachment.

For the morphological study of human urothelial cells (hUCs) and human smooth muscle cells (hSMCs), we harvested the cells at an early time point (24 h post seeding) and observed them by scanning electron microscopy (SEM). For the decellularized tracheal scaffold and the genipin-crosslinked one, hSMCs are able to attach and grow in the lumen, outer surface and edges of the tracheal scaffold (Fig. 4C). Compared with hSMCs, hUCs prefer spreading and growing in the lumen of the decellularized scaffold. On the outer surface, hUCs are spherical and contracted, which means they are not proliferating well (Fig. 4B). This can be explained by the fact that hUCs like to spread and grow on an intact luminal basement membrane, which fulfills many biological functions, including acting as a permeability barrier, influencing cellular behavior and differentiation via outside-in signaling, controlling cellular organization and tissue function, and providing structural support [66]. But for the outer surface, there are plenty of muscles without any biological constituents like collagen IV and laminin [67]. In addition, in the cartilage ring,

the cells are growing and spreading better than muscle regions, which is because the main components of the tracheal cartilage are glycosaminoglycans (GAG) and collagen that are necessary for cell attachment and repopulation. Based on the above observation, we imply that no matter where the hUCs are cultured, they will always prefer growing and proliferating on the luminal surface of the scaffold. For the decellularized trachea scaffold seeded with both hSMCs and hUCs in a mixed cell culture medium (hSMCs growth medium/ hUCs growth medium: 50/50), hSMCs are spreading and growing overwhelmingly in the lumen, outer surface, edge and cartilage rings of the tracheal scaffold, while hUCs are only able to grow in the lumen and cartilage rings of the scaffold and still prefer the luminal surface (Fig. 4D). Instead of seeding both hSMCs and hUCs in a mixed cell culture medium together, we suggest that the hSMCs should be seeded on the outer surface of the scaffold with only hSMCs growth medium and when they are able to penetrate into the tracheal scaffold, we start growing hUCs in the lumen with only hUCs growth medium.

In a mixed cell culture medium (hSMCs growth medium/ hUCs growth medium: 50/50), we also tried to seed both hUCs and hSMCs on the decellularized tracheal scaffold for four weeks. Although hSMCs are able to spread and proliferate overwhelmingly on various parts of the tracheal scaffold, the growth of hUCs declined over time, regardless of genipin-crosslinking. For immunofluorescence staining, pan-cytokeratin is a cytoskeleton marker for hUCs, while alpha-smooth muscle actin is a specific marker for hSMCs. Pan-cytokeratin is stained red for the decellularized tracheal scaffold seeded with both two cells for only three days, while there is no red staining for the scaffold after a week (Fig. 5B). As for alpha-smooth muscle actin (SMA), there is a positive staining (red) for the cell-seeded tracheal scaffold from three days to a week.

Also, we failed to grow hUCs on the outer surface of the decellularized scaffold in a mixed cell culture medium, even if we increased the time to four weeks, suggesting that hUCs are unable to attach to the tracheal scaffold filled with hSMCs and they might be removed after the first change of culture media. hUCs won't grow well *in vitro* and is a main challenge and limitation that many other investigators have encountered before, which will prevent a lot of further comprehensive experiments [42]. More studies need to be conducted to find out the mechanism behind this. For immunohistochemistry, SMA is a contractile phenotype marker; vimentin is a synthetic phenotype marker; Ki67 is a cellular marker for proliferation and cleaved caspase 3 is a marker related to cellular apoptosis. The staining of SMA and vimentin is positive in some vessel-like structures, due to the presence of some biochemical components in the decellularized tracheal scaffold (Fig. 5C, dotted circles). In addition, the positive staining of Ki67 and cleaved caspase 3 is observed, suggesting the proliferation and apoptosis of various cells. And for the NUC construction *in vivo*, since the decellularized tracheal scaffold with or without cell seeding might behave differently *in vivo*, more investigation is needed.

With quantitative real-time polymerase chain reaction (qRT-PCR), the level of gene expression for both human smooth muscle cells (hSMCs) and human urothelial cells (hUCs) were evaluated. According to Fig. 5D, we observe that the expression levels of some genes were upregulated, while some gene expressions were downregulated or not detected through one week to four weeks. The genes with increased values of expression are the markers of hSMCs, while the undetected gene and the genes with decreased values of expression are the genetic markers of hUCs. Specifically, the gene expression levels of the contractile phenotype marker (SMA) and synthetic phenotype marker (vimentin) for hSMCs were increased over time [68], which

confirmed the existence of hSMCs and revealed the decellularized tracheal scaffold was able to support the growth and proliferation of hSMCs *in vitro*. However, the growth of hSMCs *in vitro* dwindled with time, which limited our current investigation. We may need more investigations on the cell-substrate interactions under biodynamic conditions and how to resist the enzymatic degradation [69].

Chapter 5. Conclusion

In conclusion, the decellularized tracheal scaffold can be a viable alternative for constructing a neo-urinary conduit (NUC) with a combination of perfect structural flexibility and sufficient mechanical strength. In pre-clinical and clinical studies, decellularized porcine or cadaveric human tracheae are more often used because of their appropriate size and dimension. In the future, we plan to implant the decellularized tracheal scaffold with and without cell seeding into lab rats, so that we can investigate its potential translational feasibility and validations in *in vivo*.

References

[1] Langer, R., and Vacanti J.P. Tissue Engineering. Science 260, 920, 1993.

[2] Gilbert, T.W., Sellaro, T.L., and Badylak, S.F. Decellularization of tissues and organs. Biomaterials 27, 3675, 2006.

[3] Badylak SF. Xenogeneic extracellular matrix as a scaffold for tissue reconstruction. Transplant Immunol 12:367–77, 2004.

[4] Chen F, Yoo JJ, Atala A. Acellular collagen matrix as a possible ‘‘off the shelf’’ biomaterial for urethral repair. Urology 54:407–10, 1999.

[5] Dellgren G, Eriksson M, Brodin LA, Radegran K. The extended Biocor stentless aortic bioprosthesis. Early clinical experience. Scand Cardiovasc J 33:259–64, 1999.

[6] Harper C. Permacol: clinical experience with a new biomaterial. Hosp Med 62:90-5, 2001.

[7] Kolker AR, Brown DJ, Redstone JS, Scarpinato VM, Wallack MK. Multilayer reconstruction of abdominal wall defects with acellular dermal allograft (AlloDerm) and component separation. Ann Plast Surg 55:36–41, 2005.

[8] Lee MS. GraftJacket augmentation of chronic Achilles tendon ruptures. Orthopedics 27:151–3, 2004.

[9] Metcalf MH, Savoie FH, Kellum B. Surgical technique for xenograft (SIS) augmentation of rotator-cuff repairs. Oper Tech Orthop 12:204–8, 2002.

[10] Wainwright DJ. Use of an acellular allograft dermal matrix (AlloDerm) in the management of full-thickness burns. Burns 21:243–8, 1995.

[11] Parnigotto, P.P., Conconi, M.T., Gamba, P.G., and Midrio P. Experimental defect in rabbit urethra repaired with acellular aortic matrix. Urol Res 16, 28(1), 46, 2000.

[12] Atala A, Vacanti JP, Peters CA, Mandell J, Retik AB, Free-man MR. Formation of urothelial structures in vivo from dissociated cells attached to biodegradable polymer scaffolds in vitro. J Urol 148:658, 1992.

[13] Fairbanks JL, Sheldon CA, Khoury AE, Gilbert A, Bove KE. Free bladder mucosal graft biology: unique engraftment characteristics in rabbits. J Urol 148:663, 1992.

[14] Italiano G, Abatangelo Jr G, Calabro A, Abatangelo Sr G, Zanoni R, O'Regan M, Passerini Glazel G. Re-constructive surgery of the urethra: a pilot study in the rabbit on the use of hyaluronan benzyl ester (Hyaff-11) biodegradable grafts. Urol Res 25:137, 1997.

[15] Lexer E. On free transplantations. Verh Deutsch Gese Chir 40:386, 1911.

[16] Badylak, S.F., Freytes, D.O., and Gilbert, T.W. Extracellular matrix as a biological scaffold material: structure and function. Acta Biomater 5, 1, 2009.

[17] Nakamura, N., Kimura, T., and Kishida, A. Overview of the development, applications, and future perspectives of decellularized tissues and organs. ACS Biomater Sci Eng 3, 1236, 2016.

[18] Chang, Y., Tsai, C.C., Liang, H.C., and Sung, H.W. In vivo evaluation of cellular and acellular bovine pericardia fixed with a naturally occurring crosslinking agent (genipin). Biomaterials 23, 2447, 2002.

[19] Sung, H.W., Huang, R.N., Huang, L.L., Tsai, C.C., and Chiu, C.T. Feasibility study of a natural crosslinking reagent for biological tissue fixation. J Biomed Maters Res Part A 42, 560, 1998.

[20] Sung, H.W., Chang, Y., Chiu, C.T., Chen, C.N., and Liang, H.C. Crosslinking characteristics and mechanical properties of a bovine pericardium fixed with a naturally occurring crosslinking agent. J Biomed Maters Res Part A 47, 116, 1999.

[21] Bhrany, A.D., Lien, C.J., Beckstead, B.L., Futran, N.D., Muni, N.H., Giachelli, C.M., and Ratner, B.D. Crosslinking of an oesophagus acellular matrix tissue scaffold. J Tissue Eng Regen Med 2, 365, 2008.

[22] Koo, H.J., Lim, K.H., Jung, H.J., and Park, E.H. Anti-inflammatory evaluation of gardenia extract, geniposide and genipin. J Ethnopharmacol 103, 496, 2006.

[23] Suzuki, Y., Kondo, K., Ikeda, Y., and Umemura, K. Antithrombotic effect of geniposide and genipin in the mouse thrombosis model. Planta Med 67, 807, 2001.

[24] Haag, J., Baiguera, S., Jungebluth, P., Barale, D., Del, G.C., Castiglione, F., Bianco, A., Comin, C.E., Ribatti, D., and Macchiarini, P. Biomechanical and angiogenic properties of tissue-engineered rat trachea using genipin cross-linked decellularized tissue. Biomaterials 33, 780, 2012.

[25] Okada, K., Shoda, J., Kano, M., Suzuki, S., Ohtake, N., Yamamoto, M., Takahashi, H., Utsunomiya, H., Oda, K., Sato, K., and Watanabe, A. Inchinkoto, a herbal medicine, and its ingredients dually exert Mrp2/MRP2-mediated choleresis and Nrf2-mediated antioxidative action in rat livers. Amer J Physiol-Gastrointest Liver Physiol 292, G1450, 2007.

[26] Sun, F., Jiang, Y., Xu, Y., Shi, H., Zhang, S., Liu, X., Pan, S., Ye, G., Zhang, W., Zhang, F., and Zhong, C. Genipin cross-linked decellularized tracheal tubular matrix for tracheal tissue engineering applications. Sci Rep 6, 2016.

[27] Gilbert, S.M., Lai, J., Saigal, C.S., and Gore, J.L. Urologic Diseases in America Project. J Urol 190, 916, 2013.

[28] Stein, R., Schroder, A., and Thuroff, J.W. Bladder augmentation and urinary diversion in patients with neurogenic bladder: surgical considerations. J Pediatr Urol 8, 153, 2012.

[29] Shimko, M.S., Tollefson, M.K., Umbreit, E.C., Farmer, S.A., Blute, M.L, and Frank, I. J Urol 185, 562, 2011.

[30] Van der Aa, F., Joniau, S., Van Den Branden, M., and Van Poppel, H. Metabolic changes after urinary diversion. Adv Urol 764325, 2011.

[31] McDougal, W.S. Metabolic complications of urinary intestinal diversion. J Urol 147, 1199, 1992.

[32] Ferriero, M., Guaglianone, S., Papalia, R., Muto, G.L., Gallucci, M., and Simone, G. Risk assessment of stone formation in stapled orthotopic ileal neobladder. J Urol 193, 891, 2015.

[33] Okhunov, Z., Duty, B., Smith, A.D. and Okeke, Z. Management of urolithiasis in patients after urinary diversions. BJU Int 108, 330, 2011.

[34] Horst, M., Madduri, S., Goblet, R., Sulser, T., Milleret, V., Hall, H., Atala, A., and Eberli, D. Engineering functional bladder tissues. J Tissue Eng Regen Med 7, 515, 2013.

[35] de Kemp, V., de Graaf, P., Fledderus, J.O., Ruud Bosch, J.L., and de Kort, L.M. Tissue engineering for human urethral reconstruction: systematic review of recent literature. PloS one 10, e0118653, 2015.

[36] Kates, M., Singh, A., Matsui, H., Steinberg, G.D., Smith, N.D., Schoenberg, M.P., and Bivalacqua, T.J. Curr Urol Rep 16, 8, 2015.

[37] Sopko, N.A., Kates, M., and Bivalacqua, T.J. Use of regenerative tissue for urinary diversion. Curr Opin Urol 25, 578, 2015.

[38] Pokrywczynska, M., Adamowicz, J., Sharma, A.K., and Drewa, T. Human urinary bladder regeneration through tissue engineering - an analysis of 131 clinical cases. Exp Biol Med (Maywood) 239, 264, 2014.

[39] Atala, A., Bauer, S.B., Soker, S., Yoo, J.J., and Retik, A.B. Tissue-engineered autologous bladders for patients needing cystoplasty. Lancet 367, 1241, 2006.

[40] Burmeister, D., AbouShwareb, T., Tan, J., Link, K., Andersson, K.E., and Christ, G. Early stages of in situ bladder regeneration in a rodent model. Tissue Eng Part A 16, 2541, 2010.

[41] Balsara, Z.R., and Li, X. Sleeping beauty: awakening urothelium from its slumber. Am J Physiol Renal Physiol 312(4), F732, 2017.

[42] Cross, W.R., Eardley, I., Leese, H.J., and Southgate, J. A biomimetic tissue from cultured normal human urothelial cells: analysis of physiological function. Am J Physiol Renal Physiol 289, F459, 2005.

[43] Liao, W., Yang, S., Song, C., Li, Y., Meng, L., Li, X., and Xiong, Y. Tissue-engineered tubular graft for urinary diversion after radical cystectomy in rabbits. J Surg Res 182(2), 185, 2013.

[44] Sun, F., Pan, S., Shi, H.C., Zhang, F.B., Zhang, W.D., Ye, G., Liu, X.C., Zhang, S.Q., Zhong, C.H., Yuan, X.L. Structural integrity, immunogenicity and biomechanical evaluation of rabbit decellularized tracheal matrix. J Biomed Maters Res Part A 103, 1509, 2015.

[45] Baiguera S, D'Innocenzo B, Macchiarini P. Current status of regenerative replacement of the airway. Expert Rev Respir Med 5:487–494, 2011.

[46] Vogel G. Trachea transplants test the limits. Science 340: 266–268, 2013.

[47] Badylak SF, Weiss DJ, Caplan A, Macchiarini P. Engineered whole organs and complex tissues. Lancet 379:943–952, 2012.

[48] Jungebluth P, Go T, Asnaghi A, Bellini S, Martorell J, Calore C,Urbani L, Ostertag H, Mantero S, Conconi MT, Macchiarini P. Structural and morphologic evaluation of a novel detergent enzymatictissue-engineered tracheal tubular matrix. J Thorc Cardiovasc Surg 138:586–593, 2009.

[49] Go T, Jungebluth P, Baiguero S, Asnaghi A, Martorell J, Ostertag H, Mantero S, Birchall M, Bader A, Macchiarini P. Both epithelial cells and mesenchymal stem cell-derived chondrocytes contribute to the survival of tissue-engineered airway transplants in pigs. J Thorc Cardiovasc Surg 139:437–443, 2010.

[50] Partington, L., Mordan, N.J., Mason, C., Knowles, J.C., Kim, H.W., Lowdell, M.W., Birchall, M.A., and Wall, I.B. Biochemical changes caused by decellularization may compromise mechanical integrity of tracheal scaffolds. Acta Biomater 9, 5251, 2013.

[51] Batioglu-Karaaltin, A., Karaaltin, M.V., Ovali, E., Yigit, O., Kongur, M., Inan, O., Bozkurt, E., and Cansiz, H. In vivo tissue-engineered allogenic trachea transplantation in rabbits: a preliminary report. Stem Cell Rev Rep 11, 347, 2015.

[52] McGann, M.E., Bonitsky, C.M., Jackson, M.L., Ovaert, T.C., Trippel, S.B., and Wagner, D.R. Genipin crosslinking of cartilage enhances resistance to biochemical degradation and mechanical wear. J Orthop Res 33, 1571, 2015.

[53] Moll, R., Lowe, A., Laufer, J. et al: Cytokeratin 20 in human carcinomas. A new histodiagnostic marker detected by monoclonal antibodies. Am J Pathol, 140: 427, 1992.

[54] Tani A, Tada Y, Takezawa T, Wada I, Imaizumi M, Nomoto Y, Nomoto M, Omori K. Regenerative process of tracheal epithelium using a collagen vitrigel sponge scaffold. Laryngoscope 123:1469–1473, 2013.

[55] Berg M, Ejnell H, Kovacs A, Nayakawde N, Patil PB, Joshi M, Aziz L, Radberg G, Hajizadeh S, Olausson M, Sumitran-Holgersson S.Replacement of a tracheal stenosis with a tissue-engineered human trachea using autologous stem cells: a case report. Tissue Eng Part A 20:389–397, 2014.

[56] Jungebluth P, Alici E, Baiguera S, Le Blanc K, Blomberg P, Bozoky B, Crowley C, Einarsson O, Grinnemo KH, Gudbjartsson T, Le Guyader S, Henriksson G, Hermanson O, Juto JE, Leidner B, Lilja T, Liska J, Luedde T, Lundin V, Moll G, Nilsson B, Roderburg C,

Stromblad S, Sutlu T, Teixeira AI, Watz E, Seifalian A, Macchiarini P. Tracheobronchial transplantation with a stem-cell seeded bioartificial nanocomposite a proof-of-concept study. Lancet 378:1997–2004, 2011.

[57] Hong HJ, Chang JW, Park JK, Choi JW, Kim YS, Shin YS, Kim CH, Choi EC. Tracheal reconstruction using chondrocytes seeded on a poly(l-lactic-co-glycolic acid)-fibrin/hyaluronan. J Biomed Mater Res A doi: 10.1002/jbm.a.35091, 2014.

[58] Baiguera, S., Del Gaudio, C., Kuevda, E., Gonfiotti, A., Bianco, A., and Macchiarini, P. Dynamic decellularization and cross-linking of rat tracheal matrix. Biomaterials 35, 6344, 2014.

[59] Kalathur M, Baiguera S, Macchiarini P. Translating tissue-engineered tracheal replacement from bench to bedside. Cell Mol Life Sci 67:4185–4196, 2010.

[60] Porzionato, A., Sfriso, M.M., Macchi, V., Rambaldo, A., Lago, G., Lancerotto, L., Vindigni, V., and De Caro, R. Decellularized omentum as novel biologic scaffold for reconstructive surgery and regenerative medicine. Euro J Histochem 57, 4, 2013.

[61] Sung, H. W., Liang, I. L., Chen, C. N., Huang, R. N. & Liang, H. F. Stability of a biological tissue fixed with a naturally occurring crosslinking agent (genipin). J Biomed Mater Res. 55, 538–546, 2001.

[62] Kalluri, R. Basement membranes: structure, assembly and role in tumour angiogenesis. Nat Rev Cancer 3, 422, 2003.

[63] Helling, A.L., Tsekoura, E.K., Biggs, M., Bayon, Y., Pandit, A., and Zeugolis, D.I. In vitro enzymatic degradation of tissue grafts and collagen biomaterials by matrix metalloproteinases: Improving the collagenase assay. ACS Biomater Sci Eng, 2016.

[64] Takezawa, T., Ozaki, K., Nitani, A., Takabayashi, C., and Shimo-Oka, T. Collagen vitrigel: a novel scaffold that can facilitate a three-dimensional culture for reconstructing organoids. Cell Transplant 13, 463, 2004.

[65] Calderón-Colón, X., Xia, Z., Breidenich, J.L., Mulreany, D.G., Guo, Q., Uy, O.M., Tiffany, J.E., Freund, D.E., McCally, R.L., Schein, O.D., and Elisseeff, J.H. Structure and properties of collagen vitrigel membranes for ocular repair and regeneration applications. Biomaterials 33, 8286, 2012.

[66] Baiguera S, Jungebluth P, Burns A, Mavilia C, Haag J, De Coppi P, Macchiarini P. Tissue engineered human tracheas for in vivo implantation. Biomaterials 31:8931–8938, 2010.

[67] Jiang, X., Christopherson, G.T., and Mao, H.Q. The effect of nanofibre surface amine density and conjugate structure on the adhesion and proliferation of human haematopoietic progenitor cells. Interface Focus 1, 725, 2011.

[68] Beamish, J.A., He, P., Kottke-Marchant, K., and Marchant, R.E. Molecular regulation of contractile smooth muscle cell type phenotype: implications for vascular tissue engineering. Tissue Eng Part B Rev 16, 467, 2010.

[69] Singh, A., Lee, D., Sopko, N., Matsui, H., Sabnekar, P., Liu, X., Elisseeff, J., Schoenberg, M.P., Pienta, K., and Bivalacqua, T.J. Biomanufacturing seamless tubular and hollow collagen

scaffolds with unique design features and biomechanical properties. Adv Healthcare Mater 6, 2017.

[70] Singh, A., Lee, D., Jeong, H., Yu, C., Li, J., Fang, C., Sabnekar, P., Liux, X., Yoshida, T., Sopko, N., and Bivalacqua, T.J. Tissue-engineered neo-urinary conduit from decellularized trachea. Tissue Engineering Part A, 2018.

Curriculum Vitae

Education Background

Tianjin University *Tianjin, China*
Bachelor of Engineering in Pharmaceutical Engineering *Sep. 2011-Jun. 2015*
Johns Hopkins University *Baltimore, United States*
Master of Chemical and Biomolecular Engineering *Aug. 2016-May. 2018*

Research Experience

School of Chemical Engineering and Technology
Key Laboratory for Green Chemical Technology of Ministry of Education *Apr. 2014-Jun. 2015*
Advisor: Prof. Zhongyi Jiang

Project 1: Study on the Separation Properties and Interfacial Interactions Manipulation of Composite Membranes via a Mussel-inspired Approach*(Graduation Project)*

Innovation Point: to present an efficient and facile mussel- inspired approach fortailoring the membrane structure for an enhanced separation performance.

Workload:

- ✓ Prepared the ultrathin SA/PEI–PDA/PAN composition membrane by co-depositing biomimetic adhesive dopamine(DA) and polyethyleneimine (PEI) on the polyacrylonitrile (PAN) support layer and then coating with sodium alginate (SA) as the separation layer.
- ✓ Investigated the influence of the mass ratio of PEI and dopamine, reaction time, the concentration of raw material solution and temperature on the separation properties of composite membranes.
- ✓ Characterized the physical and chemical properties and structures of as-fabricated composition membranes by FESEM, FTIR, elemental analyzer, zeta-potential analyzer and contact angle goniometer, and evaluated the separation performance of composite membranes by utilizing the pervaporation dehydration of an aqueous ethanol solution as a model system.

Conclusion: The highest separation factor of the SA/PEI–PDA/PAN membranes for water/ethanol separation reaches 1807, which is 29.6 and 6.8 fold higher than those of SA/PAN and SA/PDA/PAN membranes, respectively.

Project 2: Fabrication of Layer-by-layer Self-assembly Ultrathin Hybrid Membrane for Pervaporation Dehydration

- ✓ Prepared graphene oxide (GO) dispersion following the modified Hummers methods and then characterized thephysical and chemical structures of GO by TEM, AFM, FT-IR and XRD.
- ✓ Fabricated the GO-based ultrathin hybrid multilayer membranes via layer-by-layer self-assembly of GE and GO on H-PAN membranes driven by multiple interactions by employing a home-made single-side dip-coating device, and monitored the self-assembly process by testing the zeta potential, contact angle and UV-VIS spectrum ofthe membrane surface.
- ✓ Investigated the effect of the bilayer number and operation temperature on the separation properties of hybrid membranes by measuring the pervaporation performance of GO-based membranes.

Publication

- ✓ Jing Zhao, **Chenhao Fang**, Yiwei Zhu, et al. Manipulating the interfacial interactions of composite membranes via a mussel-inspired approach for enhanced separation selectivity [J]. Journal of Materials Chemistry A, 2015, 3(39): 19980-19988.
- ✓ Jing Zhao, Yiwei Zhu, Fusheng Pan, Guangwei He, **Chenhao Fang**, et al. Fabricating graphene oxide-based ultrathin hybrid membrane for pervaporation dehydration via layer-by-layer self-assembly driven by multiple interactions [J]. Journal of Membrane Science, 2015, 487: 162-172.
- ✓ Mingshui Yao, Linan Cao, Guolin Hou, Minlan Cai, Jingwei Xiu, **Chenhao Fang**, et al. Gold–tin co-sensitized ZnO layered porous nanocrystals: enhanced responses and anti-humidity [J]. RSC Advances, 2017, 7: 20273–20280.

Internship

Fujian Institute of Research on Structure of Matter, Chinese Academy of Sciences *Jan. 2015-Feb.2015*
Project: Morphology-controlled ZnOSpherical Nanobelt-Flower Arrays and Their Sensing Properties
Advisor: Maochun Hong Academician

- ✓ Designed and selectively synthesized layered basic zinc acetate (LBZA) hierarchical structures with different morphologies from zinc acetate dehydrate ($ZnAc_2$ ▪$2H_2O$) and hexamethylenetetramine (HMT) by controlling thegrowth conditions.
- ✓ Prepared the self-standing LBZA spherical nanobelt-flower arrays films(LBZA-SFF) by immersing the silicon wafer substrate vertically in the $ZnAc_2$ and HMT mixed solution for 72h at 95℃, and heated the LBZA-SFF for 0.5h at300℃ andthen stabilized at 400℃ for 20 h to obtain the ZnO spherical nanobelt-flower arrays films(ZnO-SFF).
- ✓ Transferred the ZnO-SFF to the insulating Al_2O_3 substrate and evaluated the sensing properties to benzene gas and stability of ZnO-SFF using a home-made experiment setup.
- ✓ The introduction of Au decoration can act as a secondary sensitized element on the ZnO surface to greatly reduce the negative effect of relative humidity.
- ✓ Further studied on the sensing properties to benzene gas of ZnO spherical nanobelt-flower modified bycobaltacetate, manganeseacetate and nickel acetate, respectively.

Skill

Computer skills: C language, Origin
Professional skills: XRD, TG-DTA, SEM, FTIR,XPS, AFM,zeta-potential analyzer, elemental analyzer, contact angle goniometer, UV-VIS spectrophotometer, NMR, TEM